Monthly Notices
of the
ROYAL ASTRONOMICAL SOCIETY

Mon. Not. R. Astron. Soc. **400,** 622–628 (2009) doi:10.1111/j.1365-2966.2009.15501.x

ISO observation of molecular hydrogen and fine-structure lines in the photodissociation region IC 63

W.-F. Thi,[1⋆] E. F. van Dishoeck,[2,3] T. Bell,[4] S. Viti[5] and J. Black[6]

[1]*SUPA,† Institute for Astronomy, Royal Observatory Edinburgh, University of Edinburgh, Blackford Hill, Edinburgh EH9 3HJ*
[2]*Leiden Observatory, PO Box 9513, 2300 Leiden, the Netherlands*
[3]*Max-Planck-Institut für extraterrestrische Physik, Postfach 1312, 85741 Garching, Germany*
[4]*Downs Laboratory of Physics, California Institute of Technology 320-47, Pasadena, CA 91125, USA*
[5]*Department of Physics and Astronomy, University College London, Gower Street, London WC1E 6BT*
[6]*Onsala Space Observatory, Chalmers University, Onsala S-439 92, Sweden*

Accepted 2009 August 3. Received 2009 August 1; in original form 2009 February 12

ABSTRACT

We wish to constrain the main physical properties of the photodissociation region (PDR) IC 63. We present the results of a survey for the lowest pure-rotational lines of H_2 with the Short Wavelength Spectrometer and for the major fine-structure cooling lines of O I at 63 and 145 μm and C II at 157.7 μm with the Long Wavelength Spectrometer on board the *Infrared Space Observatory* (*ISO*) in the high-density PDR IC 63. The observations are compared with available photochemical models based on optical absorption and/or millimetre emission line data with and without enhanced H_2 formation rate on grain surfaces. The cloud density n_H is constrained by the fine-structure lines. The models include both collisional excitation and ultraviolet (UV) pumping of the H_2 ro-vibrational levels. Molecular pure-rotational lines up to S(5) are detected. The inferred column density of warm H_2 at 106 ± 11 K is $(5.9 \pm 1.8)^{+0.9}_{-0.7} \times 10^{21}$ cm^{-2}, while that of the hot component at 685 ± 68 K is $(1.2 \pm 0.4) \times 10^{19}$ cm^{-2}. Fine-structure lines are also detected in the far-infrared spectrum of IC 63. The fine-structure lines constrain the density of the PDR to be (1–5) $\times 10^3$ cm^{-3}. The impinging UV field on the PDR is enhanced by a factor of 10^3 compared to the mean interstellar field and is consistent with direct measurements in the UV. PDR models that include an enhanced H_2 formation at high dust temperature give higher H_2 intensities than models without enhancement. However, the predicted intensities are still lower than the observed intensities.

Key words: ISM: clouds.

1 INTRODUCTION

Photodissociation regions (or photon-dominated regions, PDRs) are regions of the interstellar medium where hydrogen is neutral (in the form of H I or H_2) and exposed to far-ultraviolet (FUV) radiation ($6 < h\nu < 13.6$ eV) from nearby O or B stars or from the interstellar radiation field. PDRs include diffuse clouds ($A_V < 1$ mag) and translucent clouds ($A_V < 2$ mag) as well as the skin of dense molecular clouds. In these regions, the FUV radiation field controls the thermal balance and the chemistry.

Results from the Short Wavelength Spectrometer (SWS) on board the *Infrared Space Observatory* (*ISO*)[1] have shown that the pure rotational lines of H_2 are readily detected in PDRs (Timmermann et al. 1996; Bertoldi 1997; van Dishoeck 2004). Recent observations with ground-based telescopes spatially resolved the H_2 emission in the Orion Bar (Allers et al. 2005).

Other studies have focused on observations of fine-structure lines with the Long Wavelength Spectrometer (LWS; e.g. Emery et al. 1996; Liseau et al. 1999; Vastel et al. 2001). These observations refer to molecular clouds with densities $n_H > 10^4$ cm^{-3}, exposed to intense ultraviolet (UV) radiation from nearby bright stars with an enhancement factor $I_{UV} \geq 100$ relative to the average interstellar background starlight (e.g. Draine 1978). Much less attention has been paid to the weakly illuminated clouds of lower density, which may contain a large fraction of the molecular gas in galaxies (Valentijn & van der Werf 1999). This dilute molecular gas may fill much of the volume not occupied by self-gravitating giant molecular clouds and includes the diffuse and translucent clouds that are not gravitationally bound (e.g. van Dishoeck & Black 1989; Wolfire et al. 1995). A good understanding of the physical conditions in the diffuse molecular gas is needed to determine their role in global

⋆E-mail: wfdt@roe.ac.uk
†Scottish Universities Physics Alliance.
[1]*ISO* is an ESA project with instruments funded by ESA Member States (especially the PI countries: France, Germany, the Netherlands and the United Kingdom), with the participation of ISAS and NASA.

star-forming activity and galactic evolution (e.g. McKee 1989; Li et al. 2002). The physics and chemistry of PDRs are relatively well understood and detailed models which include radiative transfer and chemistry abound in the literature (see Röllig et al. 2007, for a description of a few PDR codes).

The pure rotational lines of H_2 accessible with the *ISO*-SWS form an important new diagnostic tool of these regions as well as a test of H_2 formation efficiency at high temperature on grain surfaces. In particular, the H_2 $J = 2$ and 3 levels lie at 510 and 1015 K, respectively, and are thus excellent tracers of the warm ($\geq$100 K) gas component located in the outer layer of PDRs. Observations of H_2 rotational and ro-vibrational lines reveal that PDRs contain unexpectedly large amounts of very warm (400–700 K) molecular gas. Models of spatially resolved H_2 emissions in the Orion Bar suggest that dust attenuation or photoelectric heating should be enhanced (Allers et al. 2005).

In the outer layer of PDRs almost all of the gaseous carbon and oxygen are in the form of C^+ and O^0. Gas cooling occurs primarily by the fine-structure line emissions of O^0 ([O I] $^3P_1 \rightarrow {}^3P_2$ at 63 μm and [O I] $^3P_0 \rightarrow {}^3P_1$ at 145 μm), C^+ ([C II] $^2P_{3/2} \rightarrow {}^2P_{1/2}$ at 158 μm) and [Si II] (at 34.8 μm). The observations of the fine-structure lines constrain the density and UV field $I_{\rm UV}$. This paper presents observations of pure-rotational H_2 lines with *ISO*-SWS and of the fine-structure lines with *ISO*-LWS. The IC 63 results will be compared with those for the S140 PDR, which is thought to have a similar density and radiation field (Timmermann et al. 1996), and with recent PDR models. Thi et al. (1997) reported early results on the H_2 line emissions in IC 63.

IC 63 is a small comet-shape reflection nebula with $A_{\rm V} \simeq 7$ mag situated at a distance of ∼230 pc. It is exposed to FUV radiation ($I_{\rm UV} \approx 650$ with respect to the Draine field) from the B0.5 star γ Cas located at a distance of 1.3 pc from the cloud. The observed molecular lines in the (sub)millimetre are narrow, $\Delta V \approx 1$ km s^{-1}, indicating the absence of shocks. The size of the cloud as mapped in ^{12}CO $J = 3 \rightarrow 2$ is 40×20 arcsec^2 or 0.04×0.02 pc^2. The fact that it is isolated and nearby with a simple geometry makes it one of the simplest, best-characterized PDRs.

IC 63 has been studied intensively by Jansen, van Dishoeck & Black (1994) and Jansen et al. (1996), who observed a large variety of molecular lines to constrain the physical and chemical structure. One- and two-dimensional PDR models have been constructed by Jansen et al. (1995). The density is $\sim 5 \times 10^4$ cm^{-3} as derived from molecular line ratios and the temperature is found to decrease from ∼200 K at the edge to ∼10 K in the centre. This temperature profile reproduces well the ^{13}CO $J = 6 \rightarrow 5$ data for this cloud. Using the *International Ultraviolet Explorer* (*IUE*) satellite, Witt et al. (1989) observed the UV fluorescence of H_2 and more recently, Hurwitz (1998) detected other fluorescence lines between 900 and 1200 Å using the Berkeley spectrograph aboard the *ORPHEUS II* mission. Luhman et al. (1997) observed three near-infrared (IR) ro-vibrational H_2 emission lines. These line intensities are well reproduced by an H_2 excitation model that takes UV pumping and collisional processes into account. France et al. (2005) resolved the individual H_2 rotational fluorescence lines towards IC 63 using the far-UV satellite *FUSE*, calibrated with a rocket sounding experiment. Karr, Noriega-Crespo & Martin (2005) analysed ISOCAM circular variable filter (CVF) images of the IC 63 region. They detected strong PAHs emission as well as H_2 S(3) and S(5) emission.

The paper is organized as follows. The observations and data reduction are described in Section 2. The results for IC 63 are modelled and discussed in Section 3. The conclusions of this work are provided in Section 4.

2 OBSERVATIONS AND DATA REDUCTION

The observations were performed with the SWS grating mode SWS02 (de Graauw et al. 1996). The spectral resolving power for extended sources is 1500 at the S(0) line and 1800 and at the S(1) line, respectively. Typical integration times amount to 100 s line^{-1}. These are among the deepest integrations performed with the SWS. The H_2 lines are predicted to be weak and close to the sensitivity limit of the SWS instrument. At this level, noise caused by charged particle impacts on the detectors plays a large role. Special software designed by Valentijn & Thi (2000) has been used to handle glitches and dark current fluctuations, together with the standard Interactive Analysis Package. The flux uncertainty is of the order of 30 per cent, mostly caused by fluctuation of the dark current (Leech et al. 2001). The quality of the data varies from orbit to orbit due to the effects of 'cosmic weather'. The SWS apertures are 20×27 arcsec^2 at S(0), 14×27 arcsec^2 at S(1) and 14×20 arcsec^2 at the S(3) and S(5) lines and are considerably smaller than the LWS beams (see Table 1).

IC 63 was also observed with the LWS from 45 to 200 μm. The data presented here were taken from the *ISO* archive. The

Table 1. Lines observed by *ISO*-SWS and *ISO*-LWS.

Line	Wavelength (μm)	$E_{\rm up}/k^a$ (K)	$n_{\rm crit}{}^b$ (cm^{-3})	A^c (s^{-1})	Instr.	Beam^d (sr)
O I $^3P_1 \rightarrow {}^3P_2$	63.183	227.72	4.7 (5)	8.87 (−05)	LWS	1.3 (−7)
O I $^3P_0 \rightarrow {}^3P_1$	145.525	326	1.0 (5)	1.74 (−05)	LWS	6.65 (−8)
C II $^2P_{3/2} \rightarrow {}^2P_{1/2}$	157.740	91.22	2.8 (3)	2.4 (−06)	LWS	6.65 (−8)
H_2 S(0) 2–0	28.218	509.88	5.4 (1)	2.9 (−11)	SWS	1.3 (−8)
H_2 S(1) 3–1	17.035	1015.12	1.1 (3)	4.8 (−10)	SWS	8.9 (−9)
H_2 S(3) 5–3	9.662	2503.82	1.9 (5)	9.8 (−09)	SWS	6.6 (−9)
H_2 S(5) 7–5	6.901	4586.30	4.9 (6)	5.9 (−08)	SWS	6.6 (−9)

Note. a(b) means a $\times$ 10^b.

[a]The energy of the upper state of the transition relative to the ground state in temperature.

[b]The critical density is A/γ, where A is the Einstein-A coefficient and γ the collisional rate coefficient. The critical densities are computed assuming LTE, $T_{\rm kin} = 100$ K and the optically thin limit.

[c]Einstein-A coefficients were taken from Galavis, Mendoza & Zeippen (1997) for O I and C II and from Wolniewicz, Simbotin & Dalgarno (1998) for H_2.

[d]The LWS beam solid angles are taken from Gry et al. (2003).

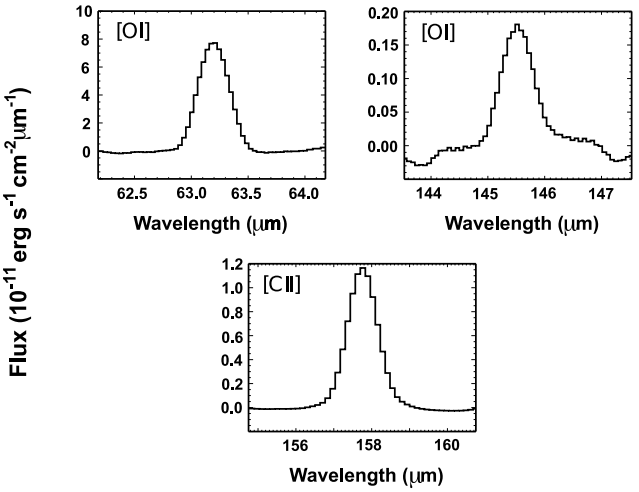

Figure 1. Continuum subtracted fine-structure [O I] and [C II] lines from IC 63 obtained with the *ISO*-LWS.

instrumental characteristics are described by Clegg et al. (1996), and the calibration of the *ISO*-LWS instrument is given by Swinyard et al. (1996). The LWS data were reduced using the Off-Line Processor, version 8.7. The LWS spectra are flux calibrated using Uranus and the photometric uncertainty is estimated to be better than 30 per cent (Swinyard et al. 1998). The spectra were obtained in grating mode at a resolving power of 250.

3 RESULTS AND DISCUSSION

3.1 Fine-structure lines

Spectra of the main cooling lines O I (63 μm), O I (145 μm) and C II (157 μm) are shown in Fig. 1. The lines are detected with high signal-to-noise ratio. Table 1 gives the parameters of the observed lines while Table 2 summarizes the measured intensities. The *ISO*-LWS C II intensity agrees quite well with that found by Keene et al. (1985) from the *Kuiper Airborne Observatory*: 1.4×10^{-4} compared with 1.0×10^{-4} erg s^{-1} cm^{-2} sr^{-1} with *ISO*-LWS. The small difference can probably be ascribed to different beam sizes. The line ratios, O I (63 μm)/C II = 1.67 ± 0.5 and O I (145 μm)/O I (63 μm) = 0.06 ± 0.02, together with the known UV field of the PDR can be used to further constrain the mean density. We have compared

Table 2. H_2 fine-structure line intensities, and continuum fluxes measured toward IC 63.

Line	Intensity (10^{-5} erg s^{-1} cm^{-2} sr^{-1})	Continuum flux
		(erg s^{-1} cm^{-2} μm^{-1})
O I $^3P_1 \rightarrow {}^3P_2$	16.9 ± 3.2[a]	20.0×10^{-19}
O I $^3P_0 \rightarrow {}^3P_1$	1.1 ± 0.2	5.5×10^{-19}
C II $^2P_{3/2} \rightarrow {}^2P_{1/2}$	10.1 ± 3.0	5.0×10^{-19}
		(Jy)
H_2 S(0) 2–0	3.0 ± 0.9[b]	2.0
H_2 S(1) 3–1	2.9 ± 0.9	1.0
H_2 S(3) 5–3	10.0 ± 3.3	0.5
H_2 S(5) 7–5	5.9 ± 1.8	0.0

[a]Errors are 2σ for the LWS data.
[b]30 per cent photometric error is assumed for the SWS data.

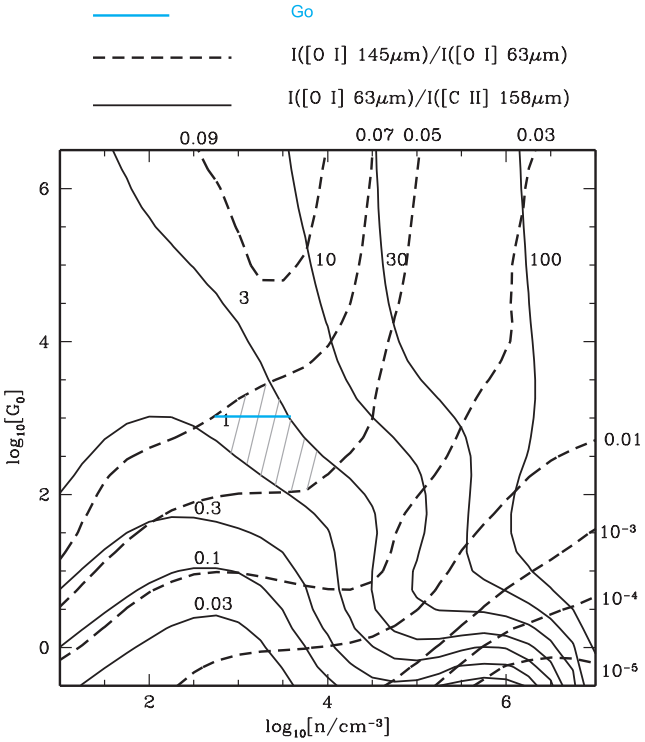

Figure 2. Contour plot of the fine-structure line ratios as functions of density and UV intensity G_0 with respect to the Habing field, adapted from Kaufman et al. (1999). The scaling factor with respect to the Draine field $I_{UV} = G_0/1.71$. The hatched area indicates the observed line ratios for IC 63. The blue line corresponds to the value of G_0 derived from UV observations.

our results to the published grid of PDR models by Kaufman et al. (1999). These calculations incorporate new collision rates for fine-structure lines and H_2, new polycyclic aromatic hydrocarbon (PAH) heating and chemistry and lower gas-phase abundances for oxygen and carbon (Savage & Sembach 1996). A turbulent broadening of 1.5 km s^{-1} was adopted, about twice that inferred from millimetre molecular lines, but Kaufman et al. argue that the results are not too sensitive to this parameter. From Fig. 2, which is an adaptation of figs 4 and 5 of Kaufman et al., the mean ratio of O I (63 μm)/C II of 1.67 ± 0.5 and O I (145 μm)/O I (63 μm) = 0.06 ± 0.02 constrain the mean density to be (1–5) × 10^3 cm^{-3} for $I_{UV} \approx 10^3$, about an order of magnitude lower than that obtained from the molecular lines (Jansen et al. 1994). The discrepancy stems mostly from uncertainties in PDR codes (Röllig et al. 2007). However, there is a possibility that the O I (63 μm) is absorbed by foreground material (Liseau 2006). An increase in O I (63 μm) will result in a higher O I (63 μm)/C II ratio and therefore a higher gas density. Alternatively, the low O I (63 μm)/C II testifies of a density gradient from cloud centre (where the molecules emit) to cloud edge (where most of the fine-structure lines are emitted).

We also modelled O I and C II intensities using the UCL PDR code (Papadopoulos, Thi & Viti 2002; Bell et al. 2005). The code has been benchmarked against a couple of PDR codes (Röllig et al. 2007). Both codes give similar results, although those from the UCL PDR code are more sensitive to the adopted turbulent velocity.

IC 63 was observed in the ^{12}CO 3–2 and 2–1 transitions by Jansen et al. (1994) with integrated temperature of 47.0 and 48.0 K km s^{-1}, respectively. We added the ^{12}CO 3–2 and 2–1 intensities observed towards IC 63 in the G_0 versus n_H diagram (see Fig. 3). The CO line and fine-structure line intensities agree relatively well.

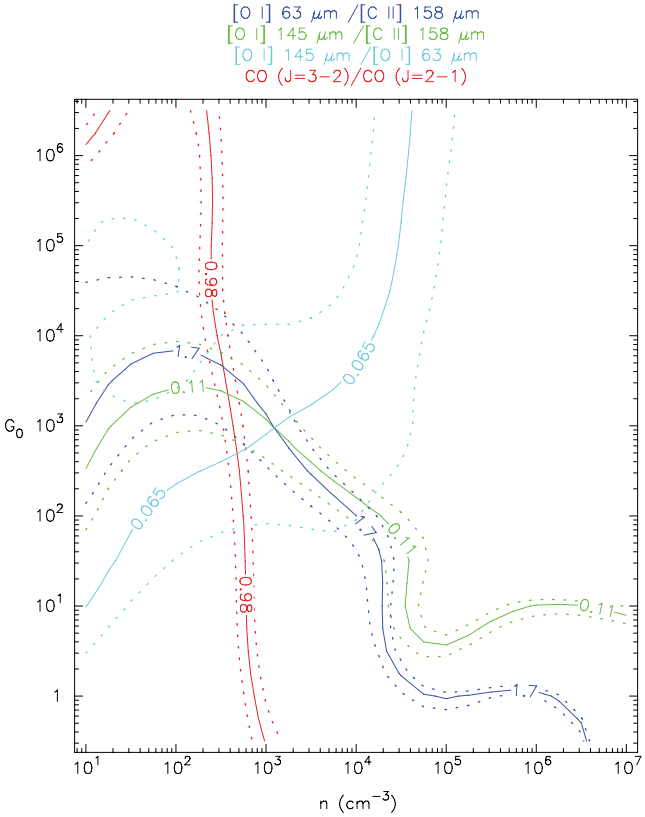

Figure 3. Contour plot of the fine-structure line ratios and CO 3–2/CO 2–1 as functions of density and UV intensity G_0 with respect to the Habing field. Figure generated using the PDR code from Kaufman et al. (1999, 2006). The solid lines are the line ratios and the dashed lines correspond to the 1σ errors.

For comparison, the O I 63 μm and C II line intensities toward the S140 PDR are a factor of 4 stronger (Timmermann et al. 1996), but the ratios are similar. This ratio mainly constrains the density of the cloud (see Fig. 2) because of the difference in the critical density between the O I 63 μm and C II lines (see Table 1).

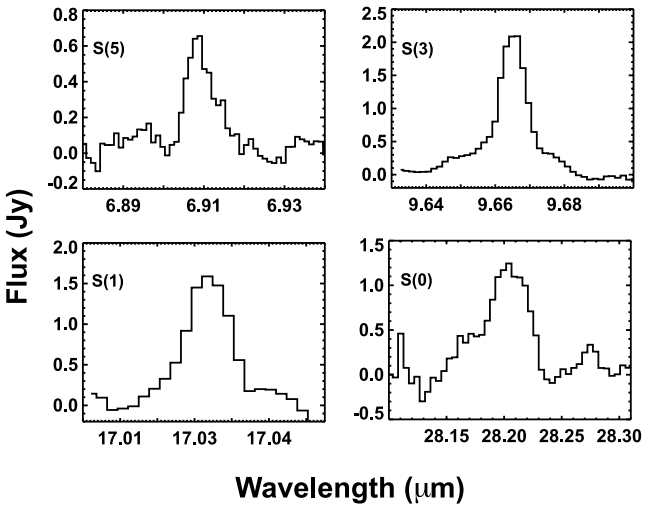

Figure 4. H_2 lines observed toward IC 63 with the *ISO*-SWS. The continuum has been subtracted.

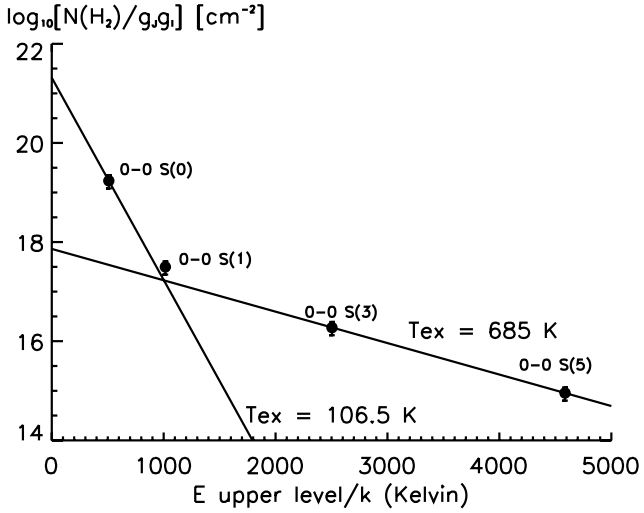

Figure 5. The H_2 excitation diagram toward the IC 63 PDR derived from the *ISO*-SWS observations.

3.2 H_2 lines

We have obtained sensitive *ISO*-SWS spectra for the H_2 lines down to (0.1–0.2) $\times$ 10^{-5} erg s^{-1} cm^{-2} sr^{-1} rms. Pure rotational H_2 lines up to S(5) are detected with *ISO*-SWS toward the peak of the CO map of IC 63 at RA (1950) $=0^{\rm h}55^{\rm m}58^{\rm s}$, Dec. (1950) $= 60^\circ37'7''$ (Fig. 4). The H_2 intensities and pseudo-continuum fluxes are summarized in Table 2. Compared with the S140 PDR, the S(5) intensity is similar, but the S(1) intensity is a factor of 6 weaker (Li et al. 2002). A small S(1) intensity means that the gas is hotter in IC 63 close to its surface. This is consistent with the smaller $I_{\rm UV}$ of 16–60 for S140 compared to IC 63. This may also suggest that geometry, especially the orientation of the Earth compared to the direction of the PDR, plays a role. Alternatively, S140 was observed at several positions and the observations may have targeted cooler regions.

3.2.1 *H_2 rotational diagram*

In the analysis of the H_2 lines, we first construct an excitation diagram, shown in Fig. 5. At local thermodynamical equilibrium (LTE) and in the optically thin approximation, the level population of level J' is related to the total column density and excitation temperature by the equation:

$$N_{J'} = N({\rm H_2}) g_I (2J'+1) \exp(-E_{J'}/T_{\rm ex})/Q(T_{\rm ex}), \quad (1)$$

where $N({\rm H_2})$ is the column density of H_2, $E_{J'}$ is the energy of the J'th rotational level expressed in kelvin, $Q(T_{\rm ex})$ is the partition function and g_I the nuclear spin degeneracy. Because the S(2) line was not observed, no constraints on the ortho-to-para ratio (OPR) can be obtained (Sternberg & Neufeld 1999), instead we adopted the OPR at LTE. The intensities are best fitted by two components of thermalized emission at temperatures of 106 ± 11 and 685 ± 68 K. The intensity of the S(1) line has nearly equal contributions from the two components. The inferred column density of warm H_2 at 106 K is $(5.9 \pm 1.8)^{+0.9}_{-0.7} \times 10^{21}$ cm^{-2}, while that of the hot component at 685 K is $(1.2 \pm 0.4) \times 10^{19}$ cm^{-2}. The errors within the parentheses take into account the uncertainties in the excitation temperature whereas the second error (for the 106 K component only) takes into account the OPR error assuming an LTE OPR population. The error introduced by the uncertainty in OPR for the hot component is negligible.

In regions with $A_V < 2$, the cooling is assumed to be predominantly caused by fine-structure emission from O I, C^+ and [C I]. From the values in Table 2, a lower limit of $(21.8 \pm 7) \times 10^{-5}$ erg s^{-1} cm^{-2} sr^{-1} on the total intensity in H_2 lines can be estimated. This intensity is comparable to, and maybe even higher than, the total intensity in fine-structure lines of (28.1 ± 6.4) erg s^{-1} cm^{-2} sr^{-1}, suggesting that the H_2 pure rotational lines are effective coolants of the edges of PDRs.

The temperature of the hot component is consistent with the ISOCAM result (630 K) but not the column density, which is a factor of ∼20 higher than in the ISOCAM study (Karr et al. 2005). The discrepancy can be mostly attributed to the choice for the continuum emission and the blend with PAH emission features in the low-resolution spectra taken by ISOCAM. The pseudo-continuum fluxes derived from the *ISO*-SWS spectra are higher than the continuum fluxes extracted from the lowest background section of the ISOCAM image. The fluxes are 0.0 and 0.5 Jy at 6.9 and 9.6 μm, respectively, for the *ISO*-SWS pseudo-continuum (Table 2) while in the ISOCAM data the continuum fluxes are at ∼0.7 and ∼1.6 Jy. Alternative possibilities include differences in beam sizes between *ISO*-SWS and ISOCAM. ISOCAM in the CVS mode has a beam size of 6 arcsec which corresponds to 6.64×10^{-10} sr, 10 times smaller than the *ISO*-SWS beam.

The total column of H_2 derived from the *ISO*-SWS spectra agrees well with the estimate of Jansen et al. (1994), $(5 \pm 2) \times 10^{21}$ cm^{-2}, although a temperature rather lower than 100 K was inferred in that analysis. The excitation temperatures characterizing levels $J = 0$–2 and $J = 3$–7 are similar to those found in diffuse molecular clouds through UV absorption line observations (e.g. Spitzer & Jenkins 1975; Rachford et al. 2002). Note that only a very small column density of hot H_2 ($T \geq 500$ K) is sufficient to produce the observed intensities of the higher lines. The hot temperature is a factor of 3 higher than the maximum kinetic temperature of ∼200 K at the edge given by the (2D) PDR models of Jansen et al. (1995). It is comparable, however, to the temperatures of 500–600 K inferred from high-J H_2 lines for other dense PDRs. As noted by Draine & Bertoldi (1996) and Bertoldi (1997), such temperatures are higher than expected from pre-*ISO* PDR models and the standard models underproduce the observed values significantly.

3.2.2 *Comparison with PDR model predictions*

As a further analysis, we compared the H_2 line ratios to the predictions from two PDR codes: the code from Kaufman et al. (1999) and the Leiden PDR code.

First, using the grid of models of Kaufman, Wolfire & Hollenbach (2006), the two line ratios H_2 S(1)/S(0) and S(3)/S(1) were used to constrain G_0 and the gas density n_H. Their models take into account both thermal and UV excitation for the H_2 level population. The observed ratios overplotted over the grid contours are shown in Figs 6 and 7 for S(1)/S(0) = 0.97 and S(3)/S(1) = 3.45, respectively. The models do not compute ratios with H_2 S(5). The H_2 S(1)/S(0) ratio is marginally consistent with the (G_0, n_H) values derived from the fine-structure and CO line ratios (Fig. 3). However, the H_2 S(3)/S(1) line ratio gives a completely different answer for G_0 and n_H. The Kaufman models can explain most observational line ratios apart form the one involving a high-J line.

We then use the Leiden PDR code. The PDR models of Jansen et al. (1995) for IC 63, which fit the H_2 UV and near-IR observations and which take into account thermal and UV excitation population of the H_2 levels, give fluxes in the pure rotational lines that are

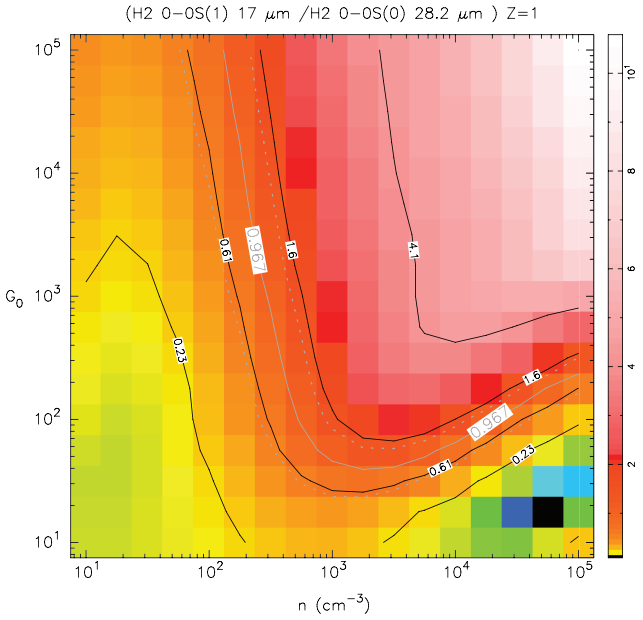

Figure 6. Contour plot of the H_2 S(1)/S(0) line ratio as functions of density and UV intensity G_0 with respect to the Habing field, adapted from Kaufman et al. (2006). The white solid contour indicates the observed ratio of 0.97 and the dashed white contours delimit the 1σ confidence region.

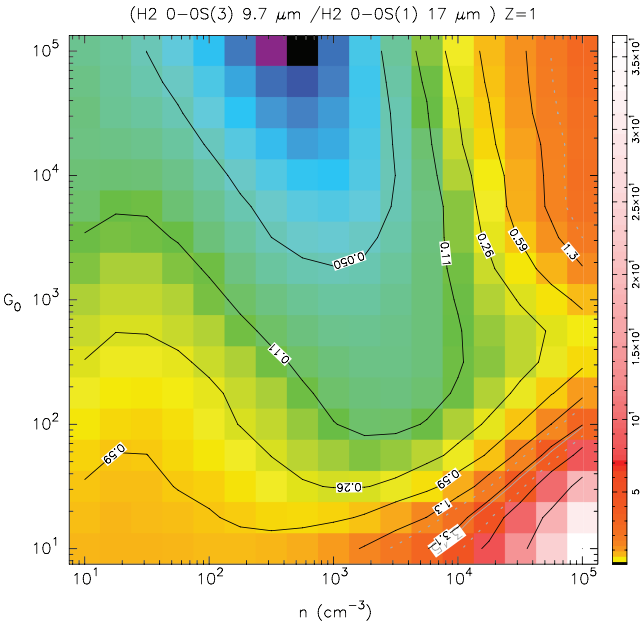

Figure 7. Contour plot of the H_2 S(3)/S(1) line ratio as functions of density and UV intensity G_0 with respect to the Habing field, adapted from Kaufman et al. (2006). The measured ratio is 3.45 and is shown in white solid contour. The 1σ confidence region is within the strip between the two dashed white contours.

up to an order of magnitude too low compared with observations. Because of the high densities, the H_2 level populations are most likely thermalized up to level 3 (see critical density in Table 1) so that the H_2 S(1)/S(0) intensity ratio directly traces the temperature structure in the warm PDR layers but the S(3)/S(1) ratio is determined by both collisions and UV pumping. Both the Leiden PDR and Kaufman PDR models fail to explain the H_2 fluxes. It should

be noticed that none of the models includes enhanced H_2 formation on grain surfaces at high temperatures.

To remedy the discrepancies between H_2 line observations and model predictions, Bertoldi (1997) and Allers et al. (2005) suggested that either the photoelectric heating efficiency needs to be increased or that the H_2 formation rate on grains needs to be larger at high temperatures, shifting the H→H_2 transition zone closer to the warm edge. Weingartner & Draine (1999) have calculated increased photoelectric heating efficiencies based on an enhanced dust-to-gas ratio in the PDR due to gas–grain drift, and Draine & Bertoldi (1996) have shown that such models can reproduce the H_2 observations of NGC 2023. Note that these comparisons include a factor of 5–10 enhancement of the models due to limb-brightening/geometry. For the case of IC 63, such effects are not expected to play a role, so that even for this simple PDR, the H_2 emission is not fully understood. The possibility of enhanced grain surface formation is discussed by Habart et al. (2004) who study the effect on increase H_2 formation rate at high temperature and find that a factor of 5 higher rate can reproduce the H_2 0–0 S(3)/H_2 1–0 S(1) ratio observed in IC 63 and other PDRs with moderate impinging UV field. The enhanced H_2 formation rate is possible at high temperature ($T > 100$ K) through a surface reaction between two chemisorbed H atoms (Cazaux & Tielens 2004).

In addition of being more abundant in the warmer PDR surface, newly formed H_2 may also be ro-vibrationally excited. However, no observational evidence of this process has been found so far (Tiné et al. 2003) and recent experiments suggest that H_2 may actually de-excite on grain surfaces before its release in the gas phase (Congiu et al. 2009).

Alternatively a cloud with a shallower temperature gradient will emit more in the lowest H_2 rotational lines. The ratio between the gas temperature derived from the two lowest rotational lines to that from the high-rotational lines can be used to test this second hypothesis. One important source of heating that may create a shallower temperature gradient is cosmic rays gas interaction. Shaw et al. (2009) manage to explain the H_2 line intensities in the Orion Bar by increasing the cosmic ray flux by a factor of a few hundred with respect to the standard value.

Finally, the warm H_2 may also be located in a region of the cloud with lower density than at the cloud centre. At low density high-J H_2 levels may be populated at non-LTE. This scenario is consistent with the lower density derived from the fine-structure lines compared to the density found using molecular lines by Jansen et al. (1995).

4 CONCLUSION

We have observed the major cooling lines with *ISO*-LWS, which have made it possible to constrain the mean density. The cloud density and impinging UV flux derived from fine-structure and CO line fluxes are consistent with model predictions and observational data at other wavelengths. We have also obtained sensitive *ISO*-SWS spectrum for the H_2 and lines from the PDR IC 63 down to (0.1–0.2) $\times 10^{-5}$ erg s^{-1} cm^{-2} sr^{-1} rms. The observed lines are stronger than computed in detailed PDR models that take collisional excitation in warm gas and UV pumping into account. This suggests that either the photoelectric heating efficiencies or the H_2 formation rate at high temperatures need to be re-examined. More efficient H_2 formation on warm grain surfaces enhance the H_2 emission but is still not sufficient. Recent studies have also explored stronger gas heating due enhanced cosmic ray fluxes, which results in stronger H_2 emission. Explanation invoked for high-density PDRs, such as geometry or gas–grain drift, do not apply to these regions. More sensitive searches for the higher rotational lines of H_2 are needed to constrain its excitation and determine the relative roles of UV pumping, collisions and the H_2 formation mechanism in establishing the level populations. Altogether, our results suggest that our understanding of the basic chemical processes of H_2 formation on grain surfaces is still incomplete. Furthermore, the density structure of IC 63 should be better constrained with high spatial resolution observations of fine-structure line emissions with the *Herschel Space Telescope*.

ACKNOWLEDGMENTS

W-FT acknowledges the financial support from the Scottish Universities Physics Alliance (SUPA). The authors wish to thank the *ISO*-SWS team for all their help in obtaining and reducing the observations. This research was supported by the Netherlands Research School for Astronomy (NOVA) and a NWO Spinoza grant.

REFERENCES

Allers K. N., Jaffe D. T., Lacy J. H., Draine B. T., Richter M. J., 2005, ApJ, 630, 368
Bell T. A., Viti S., Williams D. A., Crawford I. A., Price R. J., 2005, MNRAS, 357, 961
Bertoldi F., 1997, in Heras A. M., Leech K., Trams N. R., Perry M., eds, The First *ISO* Workshop on Analytical Spectroscopy, ESA SP-419. ESA, Noordwijk, p. 67
Cazaux S., Tielens A. G. G. M., 2004, ApJ, 604, 222
Clegg P. E. et al., 1996, A&A, 315, L38
Congiu E., Matar E., Kristensen L. E., Dulieu F., Lemaire J. L., 2009, MNRAS, 397, L96
de Graauw T. et al., 1996, A&A, 315, L49
Draine B. T., 1978, ApJS, 36, 595
Draine B. T., Bertoldi F., 1996, ApJ, 468, 269
Emery R. et al., 1996, A&A, 315, L285
France K., Andersson B.-G., McCandliss S. R., Feldman P. D., 2005, ApJ, 628, 750
Galavis M. E., Mendoza C., Zeippen C. J., 1997, A&AS, 123, 159
Gry C., di Giorgio A. M., Lorente R., Tommasi E., 2003, in Metcalfe L., Salama A., Peschke S. B., Kessler M. F., eds, The Calibration Legacy of the *ISO* Mission, ESA-SP 481. ESA, Noordwijk, p. 357
Habart E., Boulanger F., Verstraete L., Walmsley C. M., Pineau des Forêts G., 2004, A&A, 414, 531
Hurwitz M., 1998, ApJ, 500, L67
Jansen D. J., van Dishoeck E. F., Black J. H., 1994, A&A, 282, 605
Jansen D. J., van Dishoeck E. F., Black J. H., Spaans M., Sosin C., 1995, A&A, 302, 223
Jansen D. J., van Dishoeck E. F., Keene J., Boreiko R. T., Betz A. L., 1996, A&A, 309, 899
Karr J. L., Noriega-Crespo A., Martin P. G., 2005, AJ, 129, 954
Kaufman M. J., Wolfire M. G., Hollenbach D. J., Luhman M. L., 1999, ApJ, 527, 795
Kaufman M. J., Wolfire M. G., Hollenbach D. J., 2006, ApJ, 644, 283
Keene J., Blake G. A., Phillips T. G., Huggins P. J., Beichman C. A., 1985, ApJ, 299, 967
Leech K. et al., 2001, The ISO Handbooks, Vol. VI, SWS. ESA, Noordwijk
Li W., Evans N. J., Jaffe D. T., van Dishoeck E. F., Thi W., 2002, ApJ, 568, 242
Liseau R., 2006, A&A, 459, 843
Liseau R. et al., 1999, A&A, 344, 342
Luhman M. L., Luhman K. L., Benedict T., Jaffe D. T., Fischer J., 1997, ApJ, 480, L133
McKee C. F., 1989, ApJ, 345, 782
Papadopoulos P. P., Thi W.-F., Viti S., 2002, ApJ, 579, 270
Rachford B. L. et al., 2002, ApJ, 577, 221
Röllig M. et al., 2007, A&A, 467, 187

Savage B. D., Sembach K. R., 1996, ApJ, 470, 893
Shaw G., Ferland G. J., Henney W. J., Stancil P. C., Abel N. P., Pellegrini E. W., Baldwin J. A., van Hoof P. A. M., 2009, ApJ, 701, 677
Spitzer L., Jenkins E. B., 1975, ARA&A, 13, 133
Sternberg A., Neufeld D. A., 1999, ApJ, 516, 371
Swinyard B. M. et al., 1996, A&A, 315, L43
Swinyard B. M. et al., 1998, Proc. SPIE, 3354, 888
Thi W. F., van Dishoeck E. F., Jansen D. J., Spaans M., Li W., Evans N. J., Jaffe D. T., 1997, in Heras A. M., Leech K., Trams N. R., Perry M., eds, The First *ISO* Workshop on Analytical Spectroscopy, ESA SP-419. ESA, Noordwijk, p. 299
Timmermann R., Bertoldi F., Wright C. M., Drapatz S., Draine B. T., Haser L., Sternberg A., 1996, A&A, 315, L281
Tiné S., Williams D. A., Clary D. C., Farebrother A. J., Fisher A. J., Meijer A. J. H. M., Rawlings J. M. C., Davis C. J., 2003, Ap&SS, 288, 377
Valentijn E. A., Thi W. F., 2000, Exp. Astron., 10, 215
Valentijn E. A., van der Werf P. P., 1999, ApJ, 522, L29
van Dishoeck E. F., 2004, ARA&A, 42, 119
van Dishoeck E. F., Black J. H., 1989, ApJ, 340, 273
Vastel C., Spaans M., Ceccarelli C., Tielens A. G. G. M., Caux E., 2001, A&A, 376, 1064
Weingartner J. C., Draine B. T., 1999, in Cox P., Kessler M. F., eds, The Universe as Seen by *ISO*, ESA SP-427. ESA, Noordwijk, p. 783
Witt A. N., Stecher T. P., Boroson T. A., Bohlin R. C., 1989, ApJ, 336, L21
Wolfire M. G., Hollenbach D., McKee C. F., Tielens A. G. G. M., Bakes E. L. O., 1995, ApJ, 443, 152
Wolniewicz L., Simbotin I., Dalgarno A., 1998, ApJS, 115, 293

This paper has been typeset from a TEX/LATEX file prepared by the author.